Journal of Applied Electrochemistry (2006) 36:333–338
DOI 10.1007/s10800-005-9069-8

Induced electrodeposition of tungsten with nickel from acidic citrate electrolyte

S.O. MOUSSA*, M.A.M. IBRAHIM and S.S. ABD EL REHIM
Department of Chemistry, Faculty of Science, Ain Shams University, Cairo, Egypt
*(*author for correspondence, e-mail: sherif_m74@yahoo.com)*

Received 25 April 2005; accepted in revised form 12 September 2005

Key words: chronoamperometric, electrodeposition, Ni–W alloys, potentiodynamic polarization

Abstract

Induced electrodeposition of Ni–W alloys was carried out onto steel substrates from acidic citrate baths (pH 4.5) under different conditions of concentration of electrolyte, current density and temperature. Bright and highly adherent Ni–W deposits were successfully obtained with a relatively high cathodic current efficiency CCE (80–85%). The CCE increases greatly with increasing pH and Ni^{2+} ion content in the bath. The W% in the alloy deposits is in the range of 4–20 wt% depending on the operating condition. The W content in the deposit was found to increase with an increase in Ni^{2+} ion content, pH and temperature. The surface morphology was examined by scanning electron microscopy while the structure of the alloy was examined by X-ray diffraction analysis.

1. Introduction

Nickel–tungsten alloys are known for their excellent corrosion resistance [1–3], wear resistance, high hardness and magnetic properties [4, 5]. Lowe et al. [6] found that the hardness of Ni–W alloys is three times higher than that of pure electrodeposited Ni. In addition, the hardness is found to increase with increase in W content in the alloy as reported by Singh et al. [7]. It is a well-established fact that W cannot be electrodeposited from aqueous electrolytes, but can be codeposited with iron group metals such as nickel to form an alloy [8, 9]. This is classified as induced codeposition. Existing literature on the reaction mechanism varies between authors and it is contradictory. Brenner [8] presented several hypotheses such as, a catalytic influence of the cathodic surface codeposition, formation of an internal orbital complex in the electrolyte, ennobling of the deposition potential as a result of alloy deposited, formation of an active complex on the cathode, and an increase in the ''equilibrium'' solubility of W.

The electrodeposition of Ni–W alloys was carried out from different baths using either *dc* [10–13] or pulse plating techniques [14, 15]. Baths with various complexants such as maleic, gluconic, hydroxy acetic, citric and tartaric acids have been found useful for satisfactory electrodeposition [16]. However, of the many plating baths proposed for Ni–W electrodeposition, sulfamate [17] and ammonical citrate [18] are widely used. Nanostructured Ni–W alloys containing 17–22% W alloys have been electrodeposited from pH 8.5 citrate solution containing NaBr as an addition agent [19]. Recently, Wu et al. [12] investigated 2-butyne-1,4-diol as an influential factor on Ni–W codeposition. Most of the work in the literature was done at pH in the range 7.0–9.0.

The purpose of the present work was to study the electrodeposition of nickel–tungsten alloys from an acidic citrate electrolyte (pH 4.5), clarifying the factors influencing tungsten content, morphology and the alloy cathodic current efficiency. In addition, the investigation aims to throw more light on the mechanism of Ni–W codeposition from a citrate electrolyte.

2. Experimental

The Experimental setup and working procedures are the same as in the earlier publications [20, 21]. The optimum bath composition for Ni–W alloy codeposition contains: 0.3 M $NiSO_4 \cdot 7H_2O$ (nickel sulphate), 0.06 M $Na_2WO_4 \cdot 2H_2O$ (sodium tungstate), 0.05 M $C_6H_8O_7$ (citric acid) and 0.12 M $Na_3C_6H_5O_7$ (tri-sodium citrate). This is refered as NiW solution. Solutions of the same composition but without tungstate (referred to as Ni solution) or without nickel sulphate (referred to as W solution) were used for comparsion. Citric acid and tri-sodium citrate were introduced as complexing agents to form complexes with both nickel and tungsten in the bath. The required pH was obtained by adding H_2SO_4 or NaOH. All the plating baths and reagents used were made from analytical grade chemicals and doubly distilled water. For electrodeposition, a steel cathode and platinum sheet anode both of dimensions 2.5×3.0 cm were used. The percentage cathodic current efficiencies CCE% of the alloy were determined from the mass and composition of the deposited alloy and the

electrolysis charge passed [8]. The composition of the alloy was determined by an electron dispersive X-ray spectrometer, EDX (Cambridge Scanning Company Ltd.). The surface morphology of Ni–W alloy was examined using scanning electron microscopy (JEOL-JEM 1200 EX II Electron microscope). The structure of the Ni–W alloy was examined by using a Philips PW 1390 diffractometer (40 kV, 20 mV) with Ni filter and CuK_{α} radiation.

3. Results and discussion

3.1. *Potentiodynamic cathodic polarization curves*

Figure 1 shows the potentiodynamic cathodic polarization curves for the electrodeposition of nickel and for the codeposition of Ni–W alloy under similar conditions. The curve for Ni–W alloy lies at a more noble potential than the curve for Ni. On the other hand, the curve for tungsten appears due to primarily cathodic hydrogen discharge since tungsten alone cannot be deposited from pure aqueous solution [8]. The curve of Ni–W codeposition exhibits a limiting current plateau as a result of the limitation by the diffusion processes. It should be noted that Ni–W codeposition is complicated by the simultaneous discharge of hydrogen ions, which occurs both during the separate electrodeposition of nickel and during the codeposition of Ni–W alloy.

However, with the aid of the experimentally determined alloy composition over the range of current density used, the actual (calculated) partial polarization curve for each component during codeposition was computed [8]. Consequently, the polarization curve of the alloy deposition resolved into three component curves of partial current density and two of them (Ni, W) were calculated using the equation:

$$i_{\text{partial}} = i_{\text{alloy}} \times \%\ \text{metal in the alloy}$$

while the third component (H_2) was evaluated using the equation:

$$i_{H_2} = i_{\text{total}} - (i_{\text{Ni}} + i_{\text{W}})$$

The computed partial polarization curves of Ni, W and H_2 are plotted in Figure 1 (the dotted curves). It is obvious from these data that the Ni content in the deposit is expected to be always higher than that of tungsten.

It was reported [22] that at pH 4.5 nickel citrate complexes, as well as uncomplexed nickel ions (NiH_2Cit^+, NiHCit, $NiCit^-$), all coexist. The most predominant species is a mixture of NiH_2Cit^+ and NiHCit. On the other hand, tungstate forms soluble complexes with citrate ions and at pH 4.5 the chemistry of tungstate ions is rather complex. Poly-ions are formed and it is not clear how these poly-ions interact with citrate. Neverthless the equilibrium constants of different complexes of tungstate with citrate, of the type $[(WO_4)(H)_n(Cit)]^{5-n}$ are given in the literature and, at pH 4.5, the complex with $n=2$ is predominant. This is confirmed by the recent data published by Younes et al. [23] who studied the abundance of $[(WO_4)(H)_n(Cit)]^{5-n}$

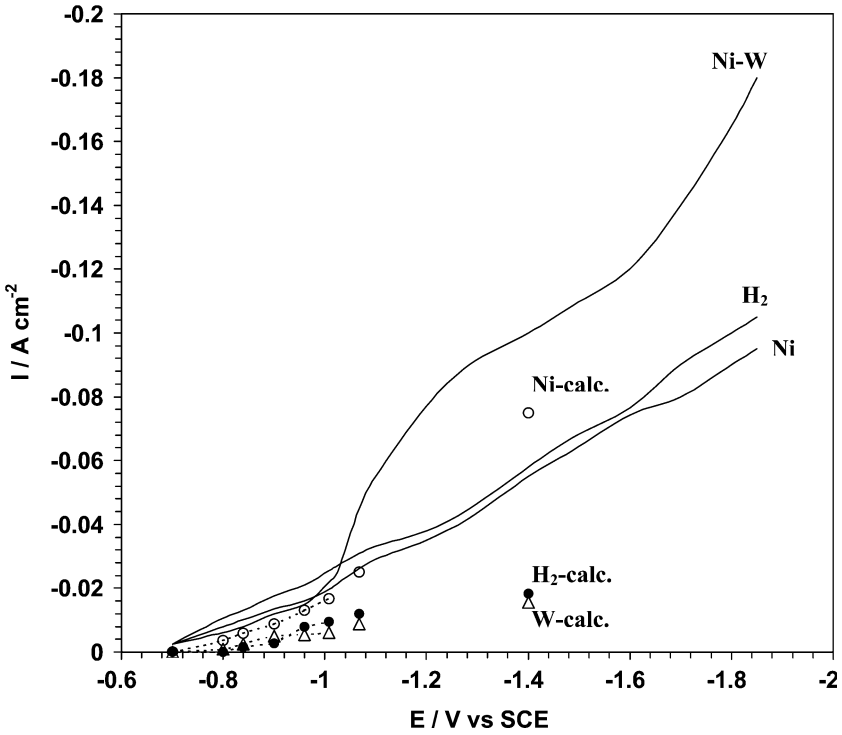

Fig. 1. Polarization curves during Ni-electrodeposition, Ni–W codeposition, H_2-reduction, from Ni solution, NiW solution, W solution respectively. The dotted lines represent the calculated curves.

complexes as a function of pH (in the range of 2.0–12.0). The data showed that at pH 4.5, only $[(WO_4)(H)_n(Cit)]^{3-}$ may be present in the solution in an acceptable amount (≈50%). However, the abundance of this complex species reached its maximum value (86%) at pH 5.5. This result confirms the increase in W% with increasing pH. The tungsten can only be codeposited (together with nickel) from this ternary complex. The existence of a ternary complex containing nickel and tungsten explains the observation that, although W is only deposited with Ni (by discharge of the ternary complex), a parallel route for deposition of Ni from its complex with citrate exists, leading to high Ni-content in the alloy.

3.2. *Cathodic current efficiency and composition of Ni–W alloys*

In most cases studied the cathodic current efficiency CCE of Ni–W alloys codeposited from acidic citrate baths is less than 100% denoting simultaneous hydrogen evolution. However, CCE is higher than that reported for some Ni–W alloys codeposited from sulfamate [17], ammonical citrate baths [18] and others [12, 23, 24]. Moreover, any plating parameter that increases the W content increases the CCE and vice versa. The effect of bath composition and some plating parameters on the overall cathodic current efficiency CCE for the alloy deposition as well as on the tungsten content in the deposits W% (wt%) were analyzed and the results are given in Figures 2–7.

Figure 2 illustrates the influence of increasing Ni^{2+} ion content in the bath on the cathodic current efficiency of the alloy codeposition as well as on W% in the deposit. At low Ni^{2+} ion concentration, the W% in the deposit is low (about 5%); however, with further increase in Ni^{2+} ion concentration, the W content in the deposit increases and reaches a maximum value of about 20%. This confirms the induced codeposition of W in the presence of Ni.

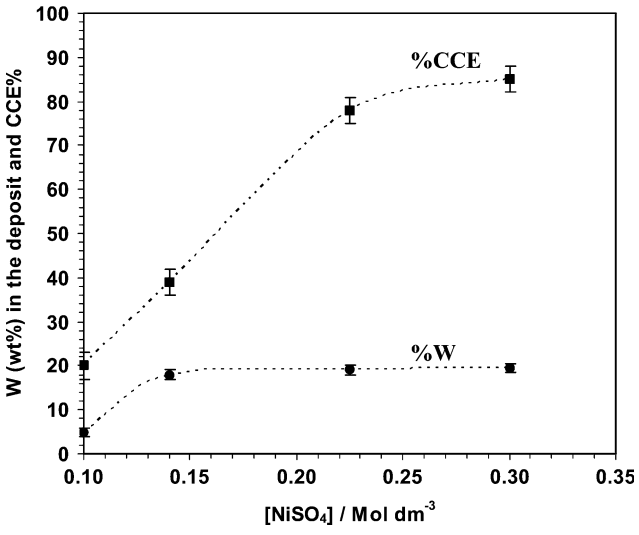

Fig. 2. Effect of $NiSO_4$ concentration on the CCE% and on W% of Ni–W alloy codeposited from NiW solution ($I = 3$ A dm^{-2}, pH 4.5, $t = 20$ min., 25 °C).

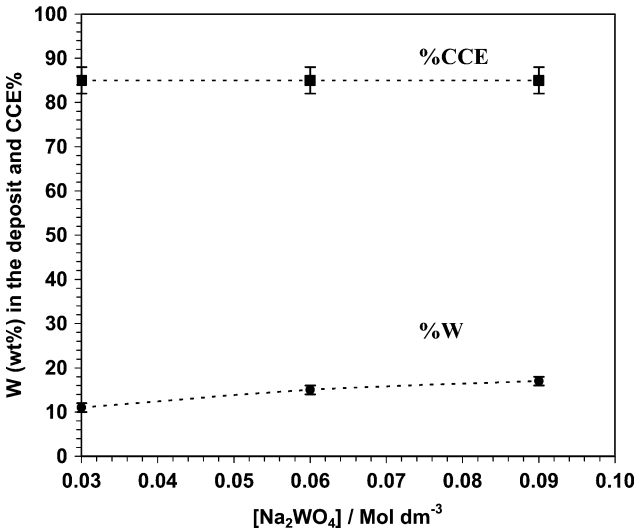

Fig. 3. Effect of Na_2WO_4 concentration on the CCE% and on W% of Ni–W alloy codeposited from NiW solution ($I = 3$ A dm^{-2}, pH 4.5, $t = 20$ min., 25 °C).

The influence of tungstate ion content in the bath on the W content in the deposit and on the CCE was studied and the results show that the W% increases from 15% to 20% by increasing the tungstate concentration from 0.03 to 0.09 M while the CCE is almost constant at 85% (Figure 3).

An increase in the total citrate concentration in the solutions, decreases the W content and the CCE of Ni–W alloy codeposition as shown in Figure 4. This is consistent with the results of Yamasaki et al. [4]. This decrease in CCE% with increasing citrate concentration may be attributed to the high stability of the ternary complex formed and, therefore, reduction from complexes is not so easy as the reduction from the simple metal ions.

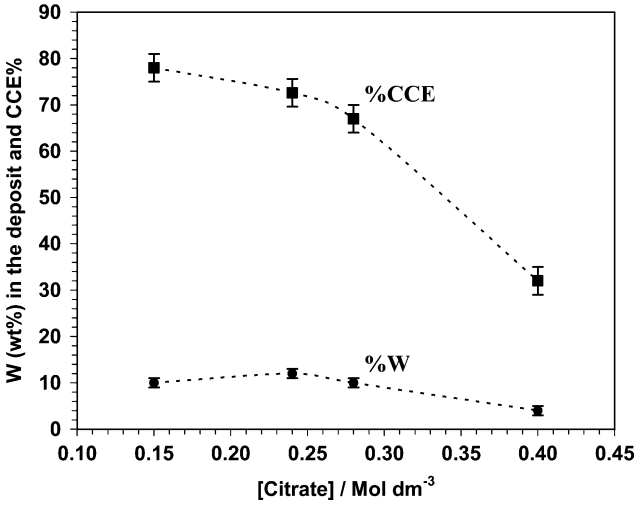

Fig. 4. Effect of citrate ion concentration on the CCE% and on W% of Ni–W alloy codeposited from NiW solution ($I = 3$ A dm^{-2}, pH 4.5, $t = 20$ min., 25 °C).

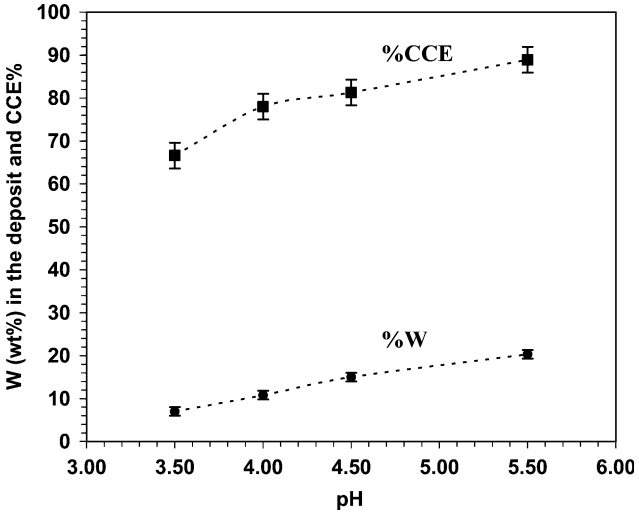

Fig. 5. Effect of pH on the CCE% and on W% of Ni–W alloy codeposited from NiW solution ($I = 3$ A dm^{-2}, $t = 20$ min., 25 °C).

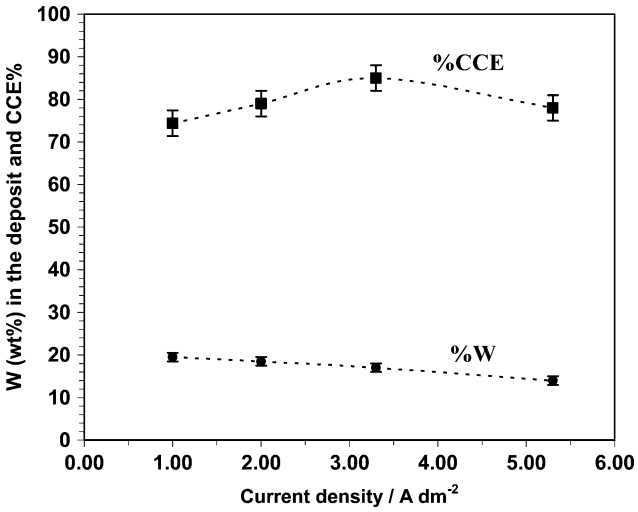

Fig. 7. Effect of current density on the CCE% and on W% of Ni–W alloy codeposited from NiW solution (pH 4.5, $t = 20$ min., 25 °C).

Figure 5 depicts the influence of pH variation of the citrate bath on the current efficiency and on W content in the deposit. It was found that the bath pH has a large effect on the CCE as well as on the W content in the deposit. For example, increasing pH from 3.5 to 5.2 increases the W content in the deposit from 9 to 25%. At the same time the CCE increases from 65 to 93%. The decrease in CCE with lowering pH may be attributed to the greater hydrogen ion concentration resulting in evolution of larger amounts of hydrogen.

An increase in bath temperature (25–65 °C) has no significant effect on the CCE (about 80%) of the alloy deposition (Figure 6). The W content in the alloy slightly increases with increasing bath temperature. This is consistent with Brenner's observations [8] and the results of Younes et al. [23]. This means that the present citrate bath might be used at ambient temperature and this could be a significant advantage in practical operations.

Figure 7 illustrates the influence of applied current density on the cathodic current efficiency CCE and on the W content in the deposit. The tungsten content is 23% at low current density (1 A dm^{-2}) and with further increase in current density the tungsten content slightly decreases and tends to level off at 20%. On the other hand, the CCE increases slightly with increasing applied current density followed by a slight decrease showing a maximum value (85%) at 3.3 A dm^{-2}.

3.3. *Chronoamperometric transients*

Chronoamperometric or current–time transients are of considerable value as a means of obtaining more information on the initial stage of nucleation and the growth mechanism for alloy deposition. For this reason, a series of chronoamperometric responses for Ni–W alloy electrodeposited from the optimum bath at different cathodic deposition potentials on a platinum

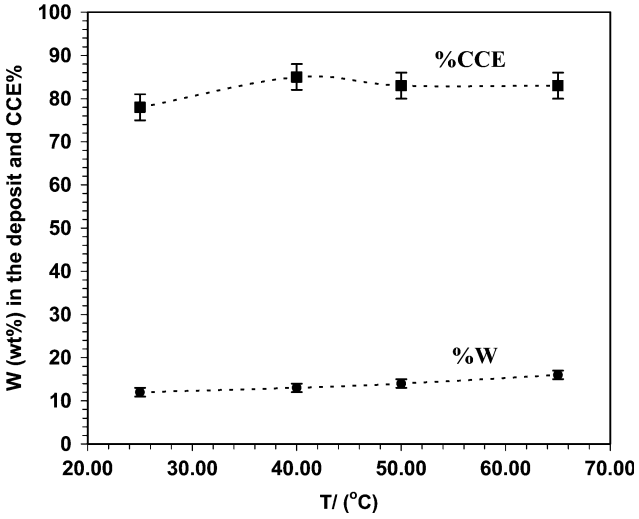

Fig. 6. Effect of temperature on the CCE% and on W% of Ni–W alloy codeposited from NiW solution ($I = 3$ A dm^{-2}, $t = 20$ min., pH 4.5).

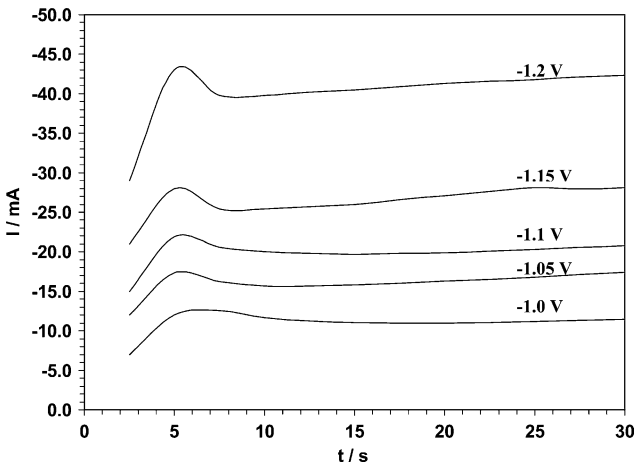

Fig. 8. Potentiostatic current–time transient curves for Ni–W alloy codeposited from NiW solution at various deposition potentials.

electrode was established. The transients are characterized by the presence of a maximum current (peak), which occurs at time t (time at which full coalescence of the crystallites occurs) (Figure 8) [25]. The presence of the maximum in the i–t curves indicates of electrodeposition of the alloy. The most interesting part of the i–t transients is the rising portion of the peak, which corresponds to the density before overlapping of the first monolayer of the growth nuclei and therefore can be used to determine the kinetics of nuclei growth [26]. Figure 9 shows a very good linear dependence of $i^{1/2}$ on time t. This type of dependence is consistent with the model of instantaneous nucleation followed by three-dimensional growth [27, 28].

3.4. *Surface morphology and X-ray analysis*

The Ni–W deposits are generally compact and have a noble appearance. Adhesion of the deposits onto steel sheets is very high since the removal of the deposit from the steel sheet is difficult. The surface morphology of the as-deposited Ni–W alloy onto steel substrates was examined by scanning electron microscopy. Figure 10 shows the morphological details of some Ni–W deposits obtained from the optimum bath. Cracks are absent on all the surfaces examined. This is due to the relatively high CCE and consequently less hydrogen evolution during deposition. It is noticable that most of the electrodeposited tungsten alloys suffer from cracking [29] because of lower CCE and high rate of hydrogen evolution during codeposition. A careful inspection of the surface morphology of the as-deposited Ni–W alloy from the optimum bath at pH 4.5 indicates that the alloy is of fibrous form as shown in Figure 10a. Recently, Donten et al. [18] reported that all electrodeposited amorphous alloys of W with iron-group metals are in fact of nanofibrous structure. On the other hand, increasing the pH from 4.5 to 6.0 retards the growth

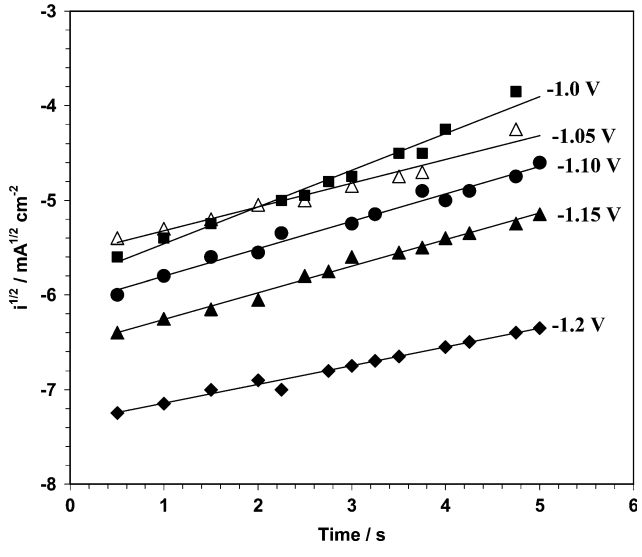

Fig. 9. Dependence of the current density $i^{1/2}$ on t for the Ni–W alloy electrodeposited from NiW solution at various deposition potentials.

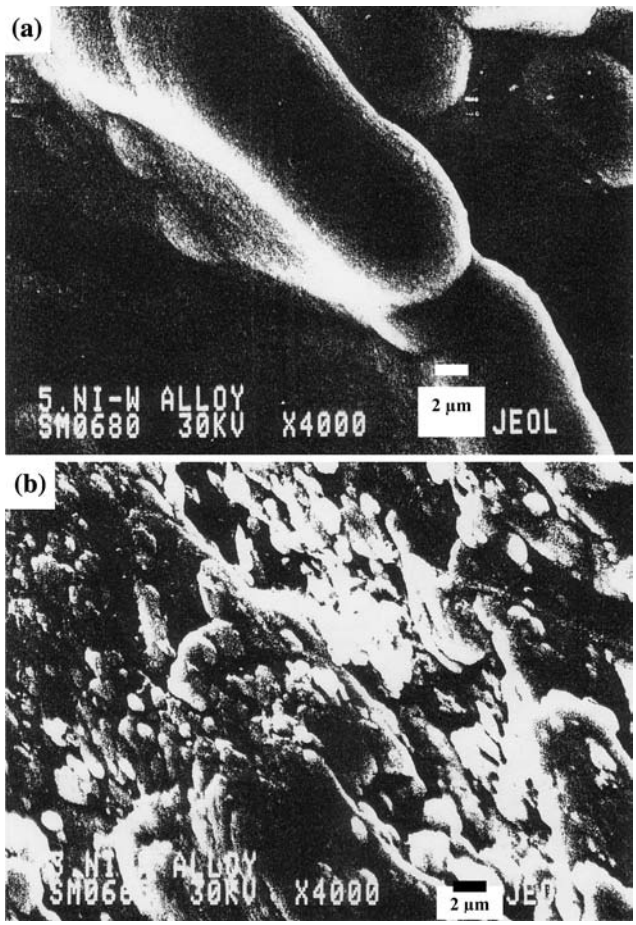

Fig. 10. Photomicrograph of Ni–W codeposited from NiW solution at: (a) $I = 3$ A dm^{-2}, pH 4.5 at 25 °C; (b) same as (a) but with pH = 6.0.

over the nucleation and high surface coverage from the fibrous-like structure is obtained. The fibres grow prependicularly to the substrate surface as shown in Figure 10b. These results are attributable to the fact that as the tungsten content in the deposit increases, with increasing pH (see Figure 4) the fibres size decreases. Therefore, the degree of surface coverage increases with increasing pH (Figure 10b).

The XRD patterns of the as-deposited Ni–W alloy (20% W) obtained onto a steel substrate are shown in Figure 11. The patterns exhibit a small shoulder at $2\theta = 42°$ corresponding to the Ni–W alloy [5, 30]. The microstructure of the Ni–W deposits exhibits (111) preferred orientration similar to the fcc (111) phase of Ni. Changing the operating conditions has no significant effect on the XRD patterns as shown in Figure 11; some authors [5, 29] have reported the formation of amorphous Ni–W alloys. However, the data shown here cannot be taken as evidence that amorphous alloys have also been deposited. The non-crystalline alloy structure must arise either because the deposition process produces mutually incoherent particles which are too small for the crystalline configuration to be formed energetically [31] or because the atoms do not bond together in the arrangement required for crystalline long-range order [30].

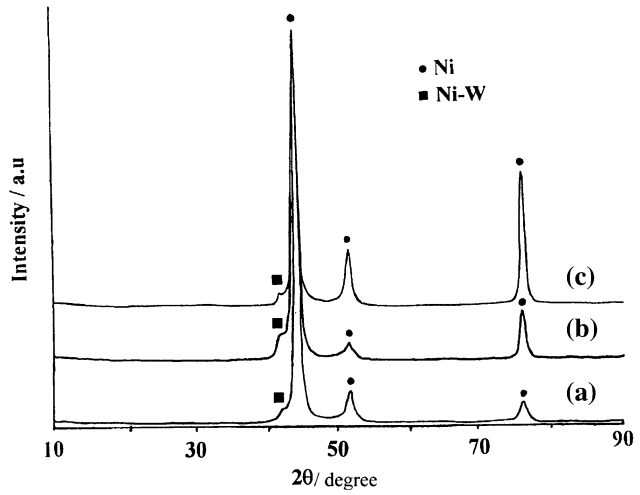

Fig. 11. X-ray diffraction analysis of as-deposited Ni–W alloy (W = 20%) onto steel substrate from the NiW solution at $I = 3$ A dm^{-2}, pH 5.0, $t = 30$ min., 25 °C.

4. Conclusion

Induced electrodeposition of highly adherent Ni–W deposits onto steel substrates from acidic citrate electrolytes was successfully achieved by using the optimum bath composition: 0.3 M $NiSO_4 \cdot 7H_2O$, 0.06 M $Na_2WO_4 \cdot 2H_2O$, 0.05 M $C_6H_8O_7$ and 0.12 M $Na_3C_6H_5O_7$. The computed partial polararization curves of Ni, W and H_2 show that the Ni content in the deposit is expected to be higher than that of tungsten in agreement with the results obtained by chemical analysis. The W% in the deposit increases with increasing Ni^{2+} ion content, pH and temperature. The cathodic current efficiency is high (80–85%). The X-ray data shows that the microstructure of Ni–W deposits exhibit (111) prefered orientation similar to the fcc (111) phase of Ni. The electrodeposition of Ni–W alloy on a platinum electrode from citrate electrolyte occurs via instantaneous nucleation followed by 3-dimensional growth as shown from the current–time transients.

References

1. M. Obradovic, J. Stevanovic, A. Despic, R. Stevanovic and J. Stoch, *J. Serb. Chem. Soc.* **66** (2001) 899.
2. M. Obradovic, J. Stevanovic, A.R. Despic and R. Stevanovic, *J. Serb. Chem. Soc.* **64** (1999) 245.
3. D.R. Gabe, *J. Appl. Electrochem.* **27** (1997) 908.
4. T. Yamasaki, P. Schlossmacher, K. Ehrlich and Y. Oginoi, *Nano-Struct. Mater.* **10** (1998) 375.
5. T. Yamasaki, *Scripta Materialia* **44**(8–9) (2001) 1497.
6. H. Lowe, W. Ehrfeld and J. Diebel, *Proc. SPIE* **3223** (1997) 168.
7. V.B. Singh, L.C. Singh and P.K. Tikoo, *J. Electrochem. Soc.* **127** (1980) 590.
8. A. Brenner, *Electrodeposition of Alloys* vol. 2 (Academic Press, New York, 1963), pp. 345.
9. A. Brenner, *Electrodeposition of Alloys* vol. 1 (Academic Press, New York, 1963), pp. 75.
10. L. Zhu, O. Younes, N. Ashkenasy, Y. Shacham and E. Gileadi, *Appl. Surf. Sci.* **200** (2002) 1.
11. K. Itoh, F. Wang and T. Watanabe, *J. Japan Inst. Metals* **65** (2001) 1023.
12. Y. Wu, D. Chang, D. Kim and S. Kwon, *Surf. Coating Technol.* **162** (2003) 269.
13. M. Donten, H. Cesiulis and Z. Stojek, *Electrochim. Acta* **45** (2000) 3389.
14. M. Donten and Z. Stojek, *J. Appl. Electrochem.* **26** (1996) 672.
15. S. Lee, Y. Lee, L. Ming and J. Chie, *Corros. Preven. Control* **46** (1999) 71.
16. R.M. Krishnan, C.J. Kennedy, S. Jayakrishnan, S. Sriveeraghavan, S.R. Natarajan and P.G. Venkatakrishnan, *Met. Finish.* **93** (1995) 33.
17. M. Bratoeva and N. Atanassov, *Met. Finish.* **96** (1998) 92.
18. M. Donten, Z. Stojek and H. Cesiulis, *J. Electrochem. Soc.* **150** (2003) C95–C98.
19. T. Yamasaki, R. Tomohira, Y. Ogino, P. Schlossmacher K. Ehrlich, *Plat. Surf. Finish.* **87** (2000) 148.
20. S.S. Abd El Rehim, M.A.M. Ibrahim, M.M. Dankeria M. Emad, *Trans. Inst. Met. Finish.* **80** (2002) 105.
21. M.A.M. Ibrahim, S.S. Abd El Rehim and S.O. Moussa, *J. Appl. Electrochem.* **33** (2003) 627–633.
22. M.A.M. Ibrahim, S.S. Abd El Rehim, S.M. Abd El Wahaab and M.M. Dankeria, *Plat. Surf. Finish.* **86** (1999) 69.
23. O. Younes and E. Gileadi, *Electrochem. Sol. State Lett.* **3** (2000) 543.
24. O. Younes, L. Zhu, Y. Rosenberg, S. Diamand and E. Gileadi, *Langmuir* **17** (2001) 8270.
25. J. Amblard, M. Froment, G. Maurin, D. Mercier and E. Trevisen-Pikacz, *J. Electroanal. Chem.* **134** (1982) 345.
26. S. Fletcher, C.S. Holliday, D. Gates, M. Westcott, T. Lwin G. Nelson, *J. Electronanal. Chem.* **159** (1983) 267.
27. C.Q. Cui, S.P. Jiang and A.C.C. Tseung, *J. Electrochem. Soc.* **137** (1990) 3418.
28. S. Swathirajan, *J. Electrochem. Soc.* **133** (1986) 671.
29. K. Wikiel and J. Osteryoung, *J. Appl. Electrochem.* **22** (1992) 506.
30. T. Nasu, M. Sakurai, T. Kamiyama, T. Usuki, O. Uemura T. Yamasaki, *J. Non-Crystalline Solids* **312–314** (2002) 319.
31. T. Omi, H.L. Glass and H. Yamamoto, *J. Electrochem. Soc.* **123** (1976) 341.